

ICONN 2015 [4th - 6th Feb 2015]

International Conference on Nanoscience and Nanotechnology-2015
SRM University, Chennai, India

Optical and electrical behavior of nanocrystalline forsterite $Mg_{2-x}Zn_xSiO_4$

B. Karthikeyan^{1*}, K. Balachandrakumar¹, K. Sakthiraj¹
and N. Rajamanickam²

¹Department of Physics, Kamaraj College of Engineering and Technology,
Virudhunagar – 626 001 India

²Physics Research Centre, VHNSN College, Virudhunagar – 626 001. India

Abstract: Forsterite (Mg_2SiO_4) nanocrystalline ceramic material is a potential candidate in the applications of laser, solid-oxide fuel cell, biomedical engineering, astrophysics, etc. It is therefore chosen in the present study and $Mg_{2-x}Zn_xSiO_4$ ($x = 0, 0.15$ and 0.25) has been synthesized with the help of high energy ball mill through mechanically activation method. The prepared samples were sintered at two different temperatures ($850^{\circ}C$ and $1000^{\circ}C$) to acquire homogeneity of the material and to achieve the proper phase transformation from the raw materials talc, periclase and the oxide of impurity element (Zn) into forsterite nanoparticle. The structural characterization of the samples was done by X-ray diffraction pattern. The optical properties were analyzed with the help of UV-VIS, FT-IR and photoluminescence (PL) spectra. It is found from the results of UV-VIS spectra that optical band gap decreases with increasing dopant concentration and also the sintering temperature. The observed IR peaks are well coincident with the characteristic peaks of forsterite in the wavenumber region $830 - 1007\text{ cm}^{-1}$. With the help of PL spectra, it is seen that luminescence effect has been improved on doping Zn with Mg_2SiO_4 . The electrical behavior of doped and undoped forsterite nanocrystalline powder was also studied over a wide range of frequency and temperature.

Keywords: Forsterite nanoparticle; XRD; UV-VIS, FT-IR, PL, impedance spectra

Introduction

It is widely known that optical and electrical characterizations are considered to be a good quality check for nanocrystalline ceramic material. There are various techniques to synthesize nanomaterials such as inert gas condensation, chemical vapor deposition, plasma arcing, electro-deposition, sol-gel, high energy ball milling, etc.¹⁻². Among these methods, high energy ball milling has many advantages because it is very simple, relatively inexpensive, applicable to any class of materials and can also be easily scaled up to large quantities³. Ball milling induces self-sustaining reactions in many sufficiently exothermic powder mixtures and the chemical reactions induced by milling or mechanical treatment are known to be very effective for the preparation of nanocrystalline powders consisting of more than two phases⁴. In the present study, the ball milling is therefore adopted for the synthesis of various samples.

Forsterite (Mg_2SiO_4) nanocrystalline material plays a vital role in many fields like electronics, biomedical engineering, astrophysics, etc. Featuring low microwave loss and extremely low electrical conductivity, forsterite can be used in electron tubes and as a substrate material in electronics⁵. The rigorous oxidation-reduction environment stability, excellent electrical insulation and high heat endurance up to 1700°C make forsterite a preferable material for the production of gaskets in solid-oxide fuel cell⁶. Forsterite can act as a potential biomaterial for prosthetic implants because of its higher fracture toughness⁷. Kioke *et al*⁸ suggested that thermo-luminescence spectra of forsterite after gamma ray irradiation were very similar to Extended Red Emission (ERE) of Red rectangle, a biconical nebula centered around a post-AGB star.

Due to the various applications of forsterite and the lack of optical and electrical properties of Zn doped forsterite in the literature, forsterite has been chosen in the present study. In this paper, we report the effect of doping on the structural properties of forsterite nanoparticle using the mechanical activation method followed by thermal treatment at different concentration of Zn. The prepared mixtures or samples have been characterized by X-ray diffraction (XRD), FT-IR, PL, UV-VIS and impedance spectra.

Experimental details and characterization procedure

The starting materials were talc (99% purity, Sigma Aldrich) and periclase (99% purity, Sigma Aldrich) for getting pure form of forsterite and were mixed in the ratio 1:5 (Sample 1). For doping Zn into forsterite, the oxide powder of doping element was added with talc and periclase in two different dopant concentrations as mentioned in table-1 (Sample 2-4). The milling was performed with the help of planetary ball mill (Retsch – PM100) for 3 hours with ball-to-powder weight ratio 9:1. After milling, heat treatment was done at two different temperatures 850°C and 1000°C for 1 hour using muffle furnace.

Table-1: Details of the samples

Sample	Dopant (Zn) concentration (in molar ratio)	Annealing temperature ($^\circ\text{C}$)
1	---	850
2	15 %	850
3	25 %	850
4	15 %	1000

The prepared samples were examined by XRD analysis using PANalytical X'Pert PRO by allowing the Cu- K_{α} beam of wavelength of 1.5406 \AA . The crystallite size (D) was determined from full-width at half-maximum (FWHM) of XRD peaks using Scherrer's equation

$$D = \frac{0.9\lambda}{\beta \cos \theta} \quad (1)$$

where λ is the wavelength of incident radiation, β is FWHM and θ is diffracting angle and the values of particle size have been given in table-2.

The IR spectra were observed using KBr pellets made from different mixtures in the region from 400 to 1200 cm^{-1} with Shimadzu IRAffinity-IS FTIR spectrophotometer. The PL spectra were also observed in the visible region using Cary Eclipse Fluorescence Spectrophotometer, by exciting the sample using the beam of wavelength 370 nm. The optical absorption spectra for all the samples were measured with the UV-VIS spectrophotometer at room temperature in order to evaluate the optical band gap and refractive index. The optical band gap of the material can be determined by using the relation⁹

$$\alpha h\nu = D(h\nu - E_g)^n \quad (2)$$

where α is the absorption coefficient, $h\nu$ is the photon energy, D is a constant, E_g is the optical band gap and $n = 1/2$ for direct allowed transition. The graph (Tauc plot) is plotted by considering the values $(\alpha h\nu)^2$ and $h\nu$. The values of E_g have been calculated by extrapolating the linear portion nearer to the main peak in the graph as shown in the figure-4. The refractive index is also calculated with the help of band gap values using the relation¹⁰

$$\frac{n_r^2 - 1}{n_r^2 + 1} = 1 - \sqrt{\frac{E_g}{20}} \quad (3)$$

The obtained values of optical band gap and refractive index for all the samples are summarized in the table-2.

Impedance measurements were carried out using HIOKI LCR meter (Model 3530-50) in the frequency range 42 Hz – 1 MHz at five different temperatures (30-100°C) and the real part of impedance (Z'), the imaginary part of impedance (Z''), phase angle (θ), dielectric loss ($\tan \delta$) were measured. The impedance of the material can be written in the complex form

$$Z^* = Z' - j Z'' \quad (4)$$

where Z' and Z'' are the real and imaginary part of impedance and the dielectric loss tangent is given by

$$\tan \delta = Z' / Z'' \quad (5)$$

The Cole-Cole plots (Z' vs Z'') and the variation of dielectric loss with frequency have been depicted in the figure-5 & 6 for the nanocrystalline forsterite samples in pure and doped form at two different annealing temperatures (850 and 1000°C). In the literature¹¹, it is found that the solubility of Zn^{2+} impurities in Mg_2SiO_4 is possible only up to 15 - 20 %. Hence, only the samples 1,2 and 4 have been chosen for the impedance analysis.

Results and discussion

Figure 1 shows the XRD pattern of forsterite and Zn-doped forsterite with different Zn concentration annealed at 850°C for 1 hour for the mixtures 1 & 2 and at 1000°C for 1 hour for the mixture 4. Several peaks corresponding to the planes (211), (131), (222), (400), (221), etc., of forsterite have been indexed by referring XRD JCPDS data file (no. 34-0189). Additionally, a strong periclase XRD peak and few weak lines of enstatite Mg_2SiO_3 are appeared on XRD pattern. However, the periclase peak has been reduced drastically by adding impurity (refer figure-1b). This clearly shows that Zn atom has successfully occupied M1 site of forsterite without changing the orthorhombic structure and the forsterite phase can be increased with reduced periclase and enstatite phases, by adding the impurity Zn.

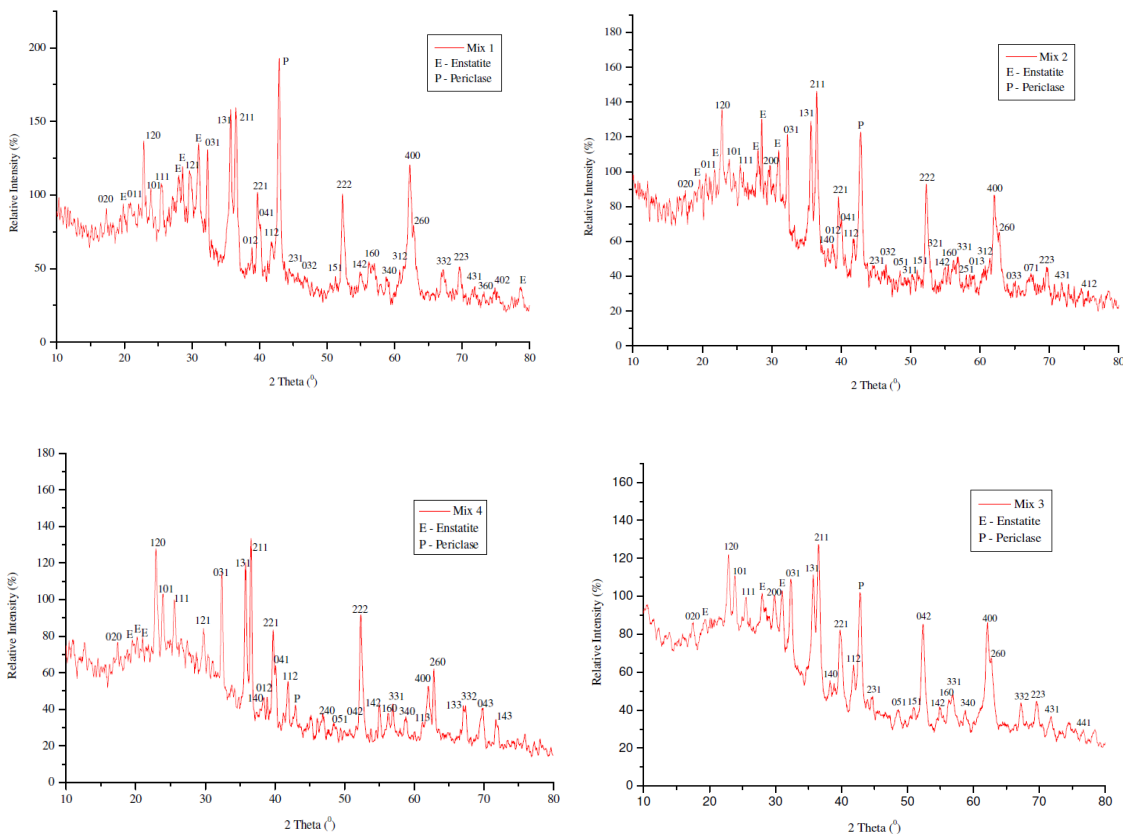


Figure-1: XRD pattern of a) Mixture 1 (Undoped); b) Mixture 2 (15% of Zn; 850°C); c) Mixture 3 (25% of Zn; 850°C); d) Mixture 4 (15% of Zn; 1000°C)

However, there is a constraint that according to Gualtlen and Bagni¹¹, a partial solid solution was observed for Zinc in forsterite and in fact, willemite was formed for Zn > 15 mol % by experiencing a change in its structure. In literature, there is no information regarding the effect of impurity Zn (except the effect of annealing temperature and milling time) on the formation of forsterite phase.

While substituting Zn ions for Mg ions, XRD trace is not showing any extra peak (for the mixtures 2 and 4) which may be due to the reason that both ions have very similar ionic radii (0.60 and 0.57 \AA for Mg and Zn respectively). Since there is no extra peak even after the addition of Zn, one can conclude that the as-grown samples are single phase and there is no change in the orthorhombic structure of forsterite.

Table-2: Particle size of as-grown samples

Sample	1	2	3	4
Particle Size D (nm)	40.90	41.58	49.45	49.13

The average particle sizes for the different mixtures have been estimated using Scherrer equation and are presented in table-2 which shows that there is no considerable change in the particle size with varying doping concentration. The FTIR spectra for undoped and two different mol % (15% and 25%) of Zn doped forsterite powder were observed in the wavenumber region $400\text{-}1200 \text{ cm}^{-1}$ and were shown in figure 5. The observed IR bands related to the characteristic peaks of forsterite appeared in the range $830 - 1007 \text{ cm}^{-1}$ corresponding to SiO_4 stretching, $500 - 620 \text{ cm}^{-1}$ for SiO_4 bending and around 420 cm^{-1} for the stretching mode of octahedral MgO_6 . It is noted that the peaks around 420 cm^{-1} have got slightly shifted towards smaller wavenumber which may be due to the accommodation of Zn ion in octahedral site. The similar effect was also observed by Lane *et al*¹² while doping Fe impurity into forsterite.

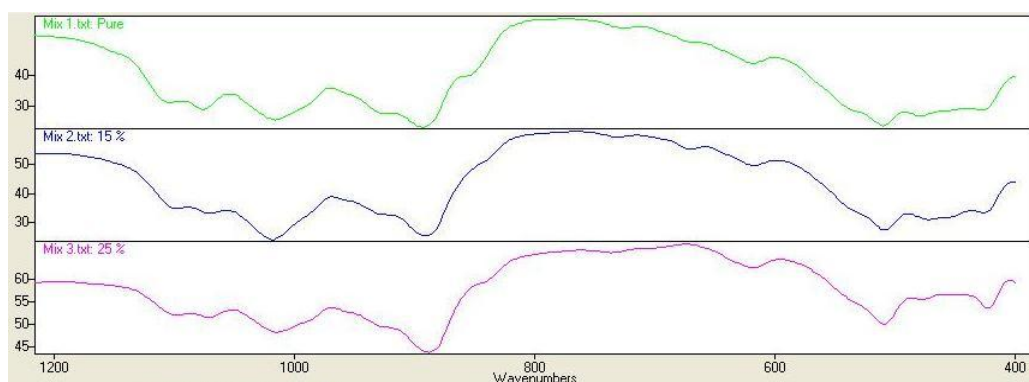


Figure-2: FTIR spectra of prepared samples

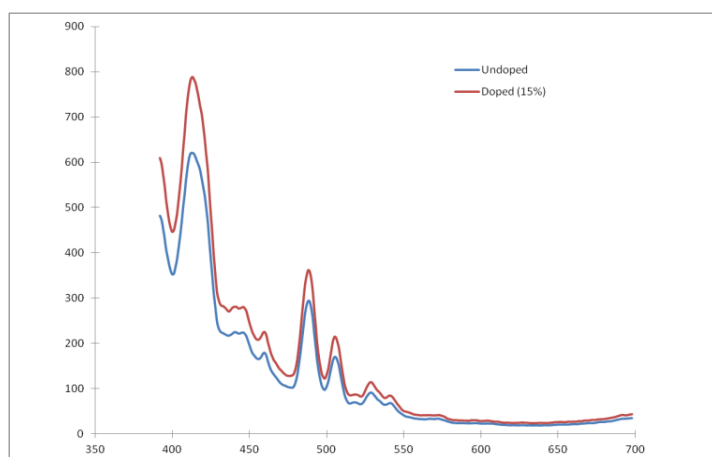


Figure-3: PL spectra of undoped and doped Mg_2SiO_4

Figure – 6 shows room temperature photoluminescence (PL) spectra of undoped and doped forsterite (i.e., for the mixtures 1 and 4) obtained by exciting the sample with UV radiation of wavelength 370 nm . Three PL emission peaks are more intense at 413.07 , 488.05 and 505.97 nm . One noticeable feature is that the PL emission intensity significantly increases with increase in dopant concentration, which could be due to doping of metallic ion in the host lattice. Thus it clears that the optical property has been enhanced on the substitution of dopants.

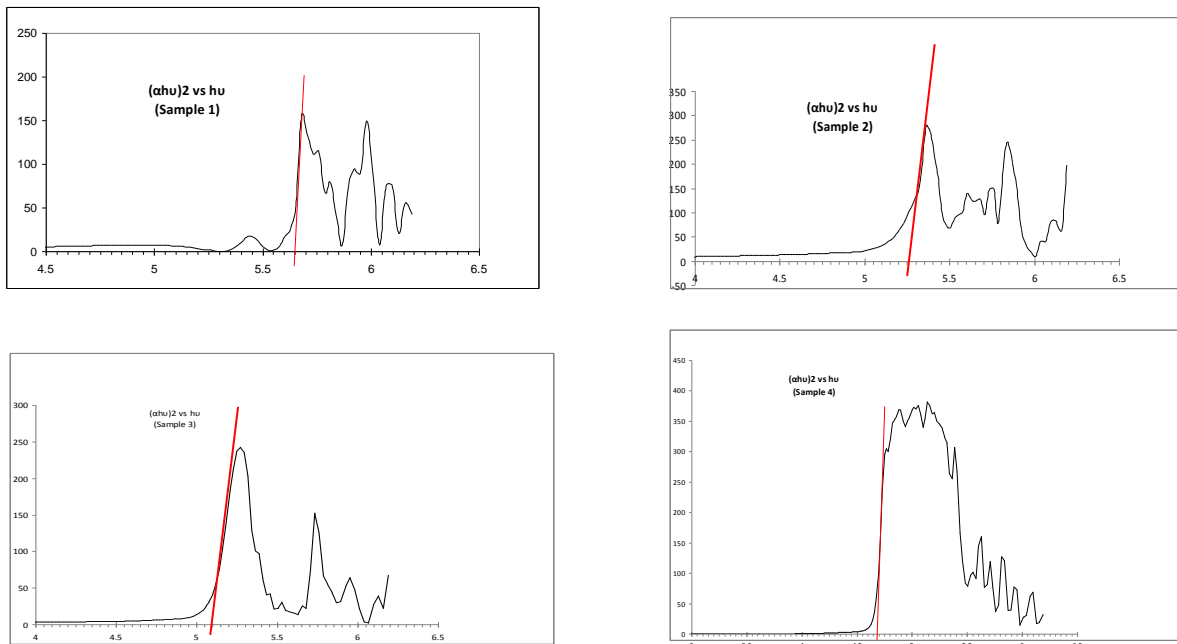


Figure-4: Tauc plot for a) Mixture 1 (Undoped); b) Mixture 2 (15% of Zn; 850⁰C); c) Mixture 3 (25% of Zn; 850⁰C); d) Mixture 4 (15% of Zn; 1000⁰C)

It is observed from the results of UV-VIS spectra that the optical band gap is increased with increasing impurity concentration and annealing temperature. This band gap narrowing may be due to the reason that the impurity Zn^{2+} band becomes broader and merges with the bottom of conduction band of forsterite. The evaluated optical band gap of the samples red shift from 5.65 to 4.65 eV as the growth temperature increased and also the concentration of the dopant atoms increased. Similar red shift of band gap was reported by Tokar Kamil *et al*¹³ when the forsterite material was doped with Fe impurities, on the basis of Mott-Hubbard picture of correlated insulators. Mamoru Kitaura *et al*¹⁴ observed the absorption spectra of α - Mg_2SiO_4 single crystal, which exhibited sharp exciton bands at 8.89, 8.70 and 9.56 eV. The present study therefore clearly shows that the particle size strongly influences the optical band gap of the material, when the crystal gets transformed from bulk to nano scale.

Table-3: Optical band gap and refractive indices

Mixture	Particle size (nm)	Optical band gap (eV)	Refractive index
1	40.90	5.65	1.909
2	41.58	5.28	1.959
3	49.45	5.10	1.985
4	49.13	4.65	2.055

Figure-5 show the variation of Z' with respect to Z'' . The variation of Z' with Z'' is linear at lower frequency, while the curves get deviated when the frequency increases. For the sample 1, the graph (fig. 5a) corresponding to 30⁰C is in the form of semicircle where as the other curves for 50, 70, 90 and 100⁰C exhibit linear variation to some extent. In the case of samples 2 and 4, the situation is entirely different, because the graph for 30⁰C is linear and the other curves are in the form of semicircle. This may arise due to the reason that the addition of impurities and the synthesis method strongly influences the impedance property of the material. The figure-6 give the information that the dielectric loss increases with increasing frequency and it is about constant at higher frequencies for all the samples. It is quite nature that the dielectric loss depends on the impurity concentration and the homogeneity of the material.

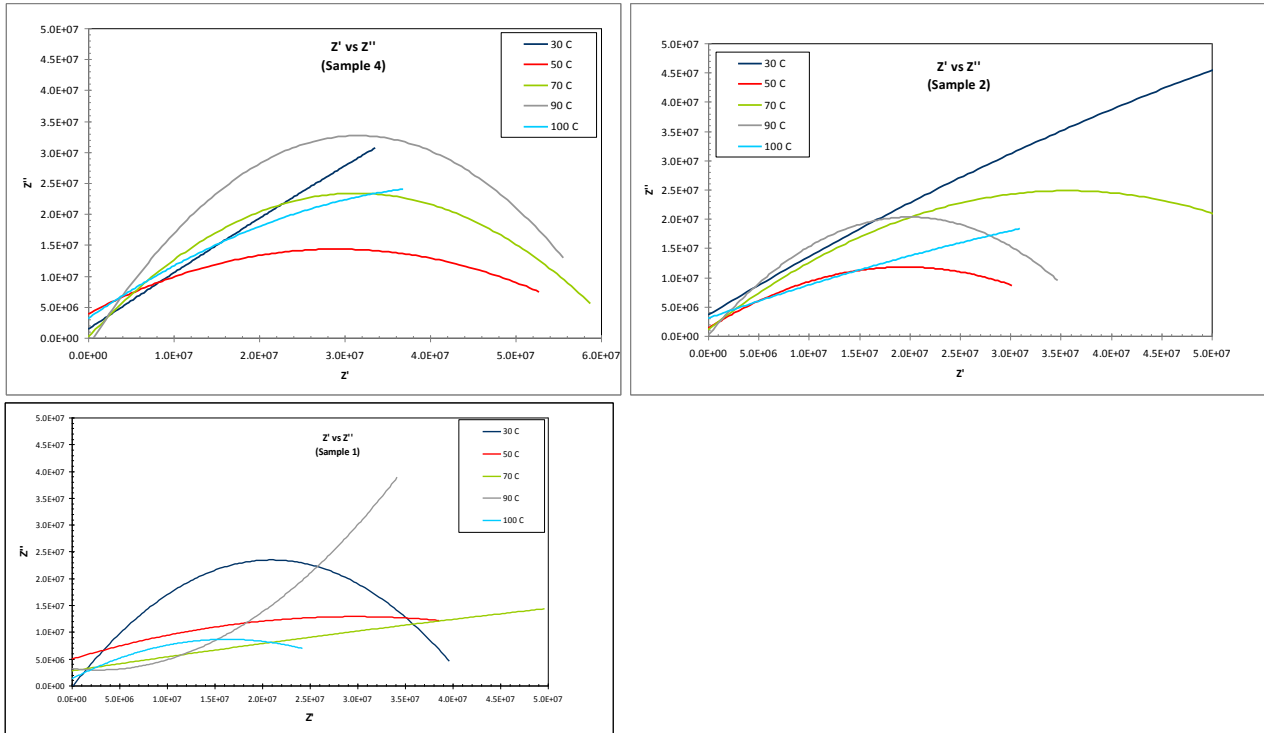


Figure-5 (a-c): Impedance (Cole-Cole) plot for the samples 1, 2 and 4 at five different temperatures

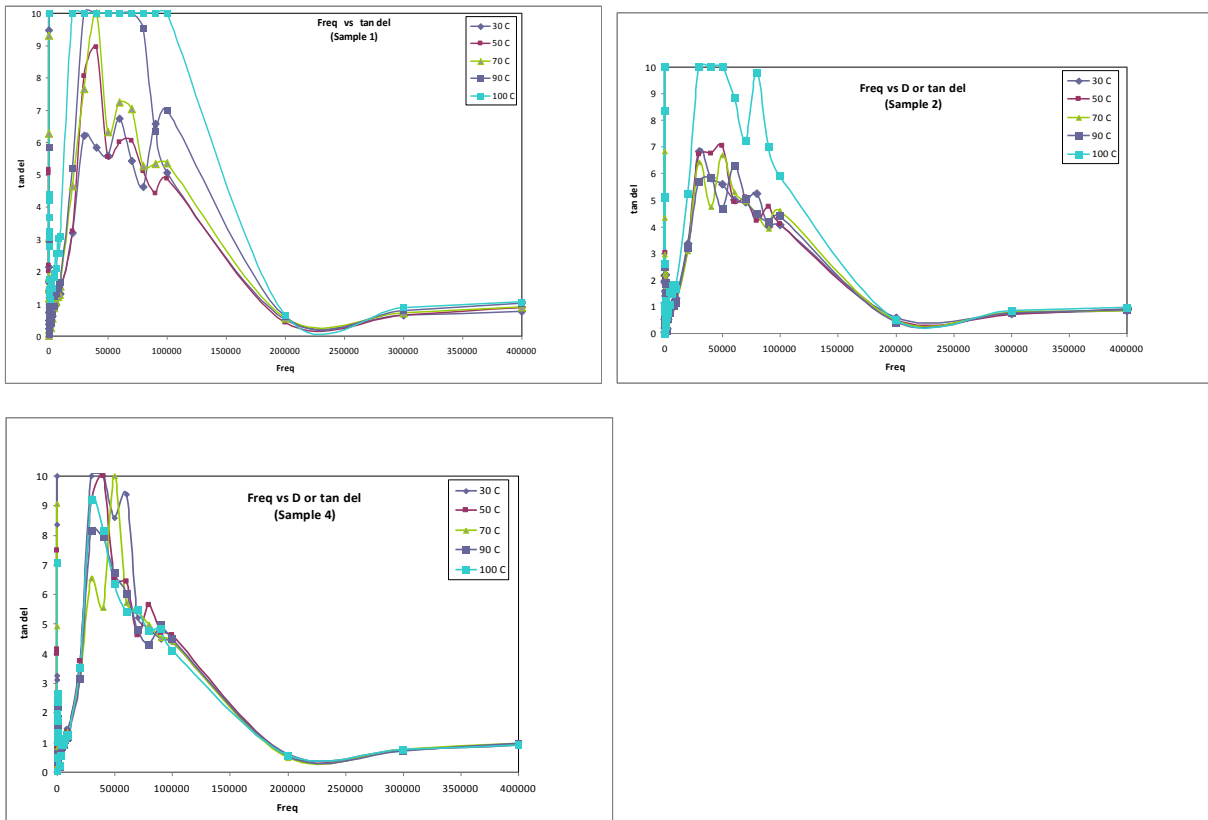


Figure-6 (a-c): Variation of dielectric loss with frequency for the samples 1, 2 and 4

Conclusion:

The present study is a first step towards the application of Zn-doped forsterite in identifying nanoclusters and thereby determining the physical conditions of astrophysical environment. It is worthy to mention here that our research team identified few suspected diatomic molecules in sunspot using spectroscopic technique¹⁵⁻¹⁶. The presence of forsterite in red rectangle is doubtful which can also be solved by doing further

analysis of doped forsterite. It is also proposed to analyze the samples with the help of thermoluminescent spectra for the application of dosimetry.

References:

1. Cao G., Nanostructures and Nanomaterials – Synthesis, properties and applications, Imperial College Press, USA, 2004.
2. Indris S. Bork D. and Heitjans P., Journal of Materials Synthesis and Processing., 2000 8(3/4), 245.
3. Baraton M.I., Synthesis, functionalization and surface treatment of nanoparticles, American Scientific Publication, USA, 2003.
4. Takacs L., Progress in Material Science., 2002, 47(4), 355.
5. Alecu I.D. and Stead. R.J., Journal of the Australian Ceramic Society., 1998, 34(2), 50.
6. Kellar J.M. Symons W. and La Barge. W.J., US Patent no. US7,785,725 B2 dated Aug 31st 2010.
7. Ramesh S. Yaghoubi A Sara Lee K.Y. Christopher Chin K.M. Purbolaksono J. Handi M. and Hassan M.A., Journal of the mechanical behavior of biomedical materials., 2013, 25 63.
8. Koike K. Chihara H. Koike C. Nakagawa M. Okada M. Matsumura M. and Takada.J., Astron. & Astrophys.,2004, 1.
9. Tauc J., Amorphous and Liquid Semiconductors, Plenum, London, 1974.
10. Sushama S.and Pradeep P., IJAPM, 2014, 4 (2), 139.
11. Gualtieri A.F. and Bagni. S., Per. Mineral., 2001 70, 27.
12. Lane M.D. Glotch T.D. Dyar M.D. Bishop J.L. Pieters C.M., Klima R. Hiroi T. and Sunshine. J.M., 40th Lunar and Planetary Science Conference (2009).
13. Tokar Kamil, Piekarz Przemyslaw, Derzsi Mariana, Jochym Pawel T., Lazewski Jan, Sternik Malgorzata Oles, Abdrzej M., Parlinski Krzysztof, Phys. Rev. B., 2010, 82 (19), 195116.
14. Mamoru Kitaura, Hideyuki Nakagawa, Akimasa Ohmishi, J. Phys. Soc. Jpn., 2002, 71, 2736.
15. Karthikeyan. B., Rajamanickam. N., Bagare. S.P., Solar Phys., 2010, 64(2): 279..
16. Karthikeyan. B., Rajamanickam. N., Bagare. S.P., Raja. V., Astroparticle Phys., 31(1): 6, 2009.
